1
2
Early age impacts of CO_2 activation on the tricalcium silicate and cement systems

3   Sean Monkman[1], Yogiraj Sargam[1], Olga Naboka[2], Barbara Lothenbach[3,4]

4   1 CarbonCure Technologies, 42 Payzant Ave, Dartmouth, NS B3B 1Z6, Canada

5   2 National Research Council Canada (NRC), 1200 Montreal Road, Ottawa, ON K1A0R6,
6   Canada

7   3 Empa Swiss Federal Laboratories for Materials Science and Technology, Laboratory
8   Concrete and Asphalt, Überlandstrasse 129, 8600 Dübendorf, Switzerland

9   4 NTNU, Department of Structural Engineering, 7491 Trondheim, Norway

10   **Abstract**

11   The early-age impacts of CO_2 activation (using a dose of 0.3% CO_2 by weight of cement)
12   on two binder systems (tricalcium silicate and cement) were studied, principally across
13   the first 3 h of hydration. The investigation included calorimetry, ICP-OES, TGA, and
14   SEM. The in-situ mineralization of CO_2 accelerated the hydration of both the systems,
15   with the effect being more pronounced in cement. During the first 30 min of hydration,
16   the CO_2 addition impacted the solution phase pH and certain elemental concentrations
17   (Ca, Mg, S). At later times of observation, the values were comparable to the level of the
18   reference sample. Thermodynamic modeling revealed that the presence of CO_2 resulted
19   in stronger undersaturation with respect to the binder phases, which implies a strong
20   driving force for their dissolution. The carbonates were observed in SEM micrographs as
21   a multitude of rhombohedral-shaped calcite crystals while TGA confirmed an increased
22   quantity of carbonates in both binder systems.

1. Introduction

Amid rising recognition of the impacts of anthropogenic global climate change and the related efforts towards implementing carbon emissions reductions, the cement and concrete industries, the source of around 7% of annual global CO_2 emissions, face the challenge of meeting a lower carbon future [1,2]. In recent years, a target of Net-Zero by 2050 [3] has inspired the industry and stakeholders to develop carbon neutrality roadmaps identifying necessary actions and potential impacts. Common among publications from ETH Zurich [4], Cembureau [5], the Portland Cement Association (PCA) [6], and the Global Cement and Concrete Association (GCCA) [7] is a recognition that action must come from across the cement-concrete value chain and that innovative technologies are needed. In the GCCA estimate, the improvements to business-as-usual approaches (increased efficiencies in cement manufacturing, concrete production, design, and construction; decarbonization of electricity; increased SCMs usage) still require carbon capture and utilization and storage (CCUS) technologies to make the largest contribution (36% of the total reduction) to reach industry net-zero goals by 2050.

The quantity of CO_2 emitted at individual cement plants suggest they hold potential as integrated links within the CCUS chain [8]. Utilization as a part of concrete production takes advantage of the mineralization pathway that it is thermodynamically favoured and offers permanent CO_2 conversion [9,10]. In contrast to other approaches for using CO_2 (e.g., conversion to fuels and chemicals, production of materials like carbon nanotubes, production of polymers), the construction materials pathway offers the greatest likelihood to make a climate impact both due to the scale of the opportunity and the advantageous energy and CO_2 footprint considerations [11].

One concept has examined the use of CO_2 as an admixture in ready mixed concrete production. Technology to add carbon dioxide into fresh concrete as part of the batching and mixing step has been developed and industrialized [12]. An optimal dose of liquid carbon dioxide is portioned and delivered according to the cement content of the batch. The CO_2, mixed into the concrete as a mixture of solid and gas, reacts with calcium ions in solution to develop calcium carbonate reaction products. Carbon dioxide reacts with

54 freshly hydrating cement to form calcium carbonate and calcium silicate hydrate gel,

55 expressed here as reactions with the main calcium silicate phases of tricalcium silicate

56 and dicalcium silicate [13]:

57

58 $3CaO \cdot SiO_2 + (3\text{-}x)CO_2 + yH_2O \rightarrow xCaO \cdot SiO_3 \cdot yH_2O + (3\text{-}x)CaCO_3$ (1)

59

60 $2CaO \cdot SiO_2 + (2\text{-}x)CO_2 + yH_2O \rightarrow xCaO \cdot SiO_3 \cdot yH_2O + (2\text{-}x)CaCO_3$ (2)

61

62 The carbonate reaction products that form are nanoscale and intermixed with calcium

63 silicate hydrate (C-S-H) gel [13–15]. The product formation has been observed to impact

64 the earliest stages of hydration, but an optimal dose does not prevent the subsequent

65 formation of typical hydration products such as calcium hydroxide, ettringite, or calcium

66 silicate hydrate gel [16].

67

68 Carbon dioxide used as a feedstock in concrete production can impart performance

69 benefits on the concrete so produced while also achieving carbon removal and reduction.

70 The in-situ nanoparticle development can improve the compressive strength of the

71 concrete. The improved strength can support a redesign of the concrete mix to use less

72 Portland cement; the approach can reduce the concrete's carbon footprint and drive

73 sustainable production [12,17]. The cement has a carbon footprint around 0.863 tonnes

74 CO_2/tonne of cement [2]. Leveraging the CO_2 utilization to use cement more efficiently

75 drives lower carbon concrete while also achieving an economic saving for the producer.

76

77 Earlier work examined adding CO_2, as an admixture, to tricalcium silicate and identifying

78 the rapid in-situ development of reaction products [14]. The present work focussed

79 attention, for the first time, on the earliest stages of hydration where the mineralization of

80 CO_2 is completed, and direct impacts are the most noticeable. Both C_3S (tricalcium

81 silicate, in cement chemistry notation) and cement were examined. An initial

82 experimental program was undertaken to determine the sensitivity of water-cementitious

83 ratio and CO_2 dose on the calorimetric response. The samples prepared with the selected

84 dose were thereafter analyzed for changes in hydration. A variety of characterization

3

85 techniques, including isothermal calorimetry, TGA, XRD, and SEM, were employed for

86 this purpose. A novel examination of the pore solution pH and solution chemistry through

87 ICP-OES identified the impacts of the CO_2 addition in both the simple C_3S system and

88 the more complex cement system. The saturation indices of various reactant and product

89 phases were determined using thermodynamic modeling. Quantities and morphologies of

90 the CO_2 mineralization and hydration products were determined. The present work

91 improves the physicochemical understanding, from the early moments of hydration, of

92 using CO_2 as a concrete admixture and how it can impart performance benefits in ready

93 mixed concrete production.

94

95 **2. Materials and methods**

96 **2.1 Materials**

97 The materials used in this study were calcium trisilicate (C_3S), cement, CO_2, and water.

98 C_3S powder was obtained from CTL Group (Skokie, IL). The cement was a general use

99 (GU) Portland cement (Table 1). The CO_2 gas (Coleman, Grade 4.0, purity 99.9%) used

100 in the study was commercial grade and supplied by BOC gases. Ultrahigh purity water,

101 ddH_2O (resistivity of 18.2 MOhm at 25 °C), was prepared in a Simplicity UV water

102 purification system (EMD Millipore Sigma). Isopropanol (HPLC grade) and HNO_3

103 (15.8N, ACS grade) were obtained from Fisher Scientific. The flowmeter (Omega

104 FMA1814A) was used to control the flow of gaseous CO_2. Analytical paste samples were

105 prepared in 20 ml scintillation vials. The paste was premixed with a vortex vial mixer

106 (Maxi Mix II, from Thermo Scientific, Pittsburgh, PA). A 50 ml plastic syringe with

107 attached 0.45 μm filter unit and Durapore PVDF membrane (Millex HV) was used to

108 extract pore solution aided by a pneumatic press.

109

110

Table 1: Chemical analyses of the cement used in the study (phases reported as weight percent, potential phase composition via calculation, cement compounds reported using cement chemistry notation)

Component	Amount
CaO	61.9%
SiO_2	19.4%
Al_2O_3	4.9%
SO_3	3.9%
Fe_2O_3	3.3%
MgO	2.7%
Free CaO	1.1%
Insoluble residue	0.45%
Total alkali as Na_2O	0.64%
Loss on ignition	2.3%
C_3S (calculated)	56%
C_2S (calculated)	14%
C_3A (calculated)	7%
C_4AF (calculated)	10%
Blaine Fineness	364 m^2/g

114

115

2.2 Sample preparation

116

117   Fig. 1 shows the experimental design adopted in this study. Additional details are

118   included in Section 1 of the Supplemental Information. A preliminary study optimized

119   the experimental conditions. Firstly, cement paste samples were prepared at different

120   water-to-cement (w/c) ratios (0.5, 0.8, 1.0, 1.2, and 1.5). A series of tests were conducted

121   to optimize the amount of pore solution extracted using the filter press. The work

122   identified an optimum w/c of 1.2 (detailed information in Section 2 of the Supplemental

123   Information) that was used for further sample preparation. Using a vortex mixer, paste

124   samples activated with CO_2 were then prepared in the following fashion: (1) portioning

125   water and cement into a vial and premixing for 30 s; (2) pause for 5 s; (3) restart mixing

126   and commence injection of the required amount of CO_2; and (4) complete CO_2 injection

127   and continue mixing until a total elapsed time of 90 sbeyond in the initial contact of the

128   water and the C_3S or cement. The samples were then transferred to an isothermal

129   calorimeter, and the gathered data was analyzed to select an optimum amount of CO_2

130   from various dosages used (0.1, 0.3, 0.5, 0.7, and 0.9% by weight of cement).

131
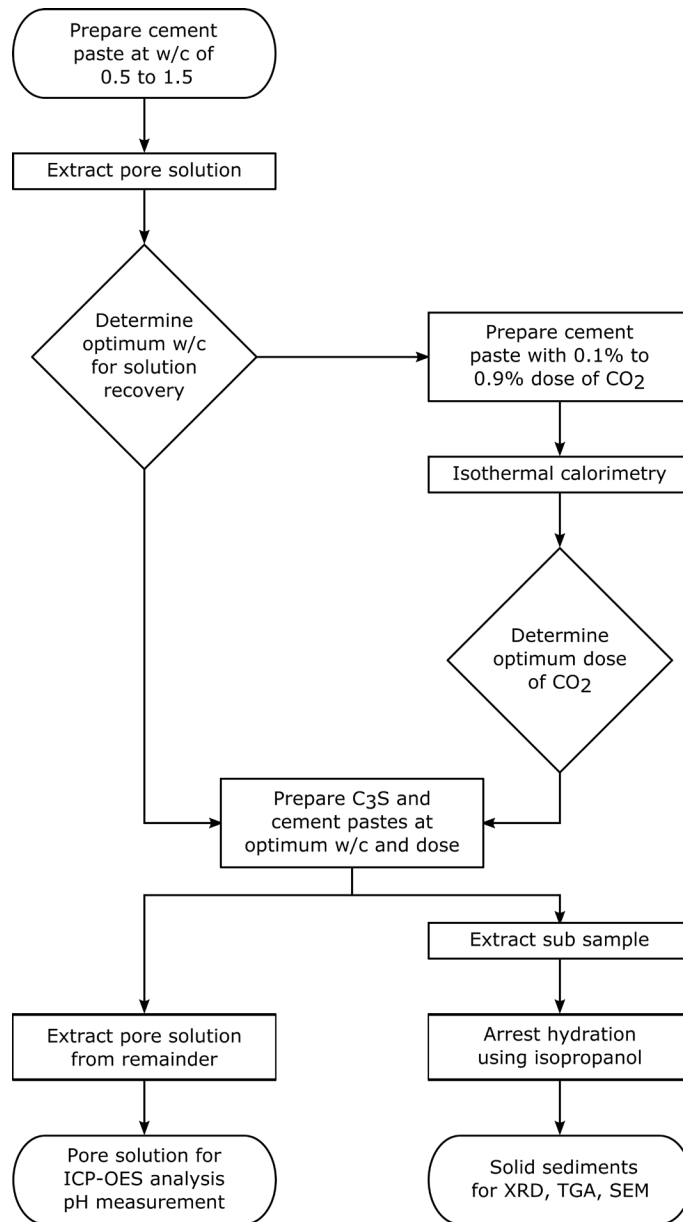
132   **Fig. 1. Experimental design used in this study**

133

134   At the determined optimums of w/c and CO_2 dose, the cement and C_3S paste samples

135   were then prepared for further analysis according to the mixing procedure. The samples

136   were let to hydrate, capped, in their vials until the required hydration arrest times. The

137   CO_2 activated system was analyzed at 1, 3, 6, 10, 15, 30, 60, 120, 180 min after the

138   conclusion of the mixing, while the control was examined at 6, 15, 30, 60, 120, and 180

139   min. At the intended time of hydration arrest, around 2 ml of paste (cement or C_3S

140   dispersion) was pipetted and transferred to a glass vial filled with about 18 ml of

141   isopropanol to arrest hydration. Solids were let to sediment for 2 to 3 min, after which the

142   vial was filled with fresh isopropanol. The sedimentation and replenishing of isopropanol

143   were repeated at least four more times to eliminate the water. The isopropanol was then

144   decanted, and the sediment-containing vial was placed in a vacuum oven equipped with a

145   liquid nitrogen trap and held at 40 - 50 °C (a temperature low enough to avoid

146   decomposition of phases such as ettringite) to dry the material. The solid sediments thus

147   obtained were used for TGA, XRD, and SEM analysis. For the ICP-OES and pH

148   measurement, pore solution was extracted using the filter press assembly.

149

150   **2.3 Test methods**

151   **2.3.1 Isothermal calorimetry**

152   Isothermal heat conduction calorimetry was performed with a TAM Air (Thermometric)

153   calorimeter. Paste samples were placed in 20 ml plastic Wheaton vials. Each sample for

154   calorimetry contained 8.8 g of paste (equivalent to 4 g of cement or C_3S). The test was

155   run at 20 °C for 24 - 48 h.

156

157   **2.3.2 TGA**

158   Thermal gravimetric analysis (TGA) was performed with SDT Q600 (TA instruments).

159   Samples (33 - 37 mg) were placed in the alumina crucible and heated to 1000 °C at a rate

160   of 10 °C/min in a nitrogen flow. Samples at the early stage of hydration showed very low

161   weight loss, which can possibly result in high errors due to weight drifts occurring during

162   the heating. Weight loss occurring during the decomposition of cement or C_3S

163   components was quantified across defined temperature intervals as per the approach of

164 Bhatty [18]. The temperature intervals were selected according to the observed onset

165 points of the calcium hydroxide and carbonate mass losses. Further analysis of the

166 carbonate loss was completed using the derivative thermogravimetric (DTG) data

167 (derivative weight (%/min) vs. temperature) to understand overlapping mass losses of

168 amorphous and crystalline carbonate. The processing of the overlapping mass losses was

169 performed with the peak fitting software Fityk [19].

170

171 **2.3.3 XRD**

172 Powder X-ray diffraction (XRD) was performed with Bruker D8 Advance diffractometer

173 equipped with position-sensitive detector Våntec-1. Radiation was generated with an X-

174 ray tube with a Cu anode (Kα radiation, λ=1.54184 Å) at 35 kV and 40 mA. The 2θ range

175 was 10 - 50°, and the resolution was 0.035°, with 2 s averaging time per step. Phase

176 analysis was performed using ICDD PDF-2 databases. The XRD did not elucidate

177 significant differences between the samples over the analysed timeframe and is included

178 in Section 7 of the Supplementary Information.

179

180 **2.3.4 SEM**

181 Scanning Electron Microscopy (SEM) was performed with a Hitachi S4800 field

182 emission scanning electron microscope with embedded Oxford Inca X'sight Energy

183 Dispersive Spectrometer (EDS) equipped with Si (Li) detector and ATW detector

184 window. Before imaging, samples were attached with double-sided conductive glue tape

185 on an aluminum sample holder without any further conductive coating. The imaging was

186 performed in secondary electron (SE) mode at 1.0 - 2.0 kV accelerating voltage. EDS

187 was performed at 8 kV accelerating voltage.

188

189 **2.3.5 ICP-OES and pH**

190 The extracted pore solution was analyzed to determine the solution phase composition.

191 The pH was measured with combination pH electrode with built in automatic temperature

192 compensation probe (Ag/AgCl reference, single junction), Accumet from Fisher

193 Scientific. To stabilize the solution and prevent precipitation, 0.4 ml of HNO_3

194   ($V_{HNO3}:V_{water} = 1:2$) was added to a 9 ml sample of pore solution. Elemental composition

195   results were corrected to the amount of HNO_3 according to: $C_{actual} = C_{laboratory} \times 9.4/9.0 =$

196     $1.044\ C_{laboratory}$. The solution was subsequently analysed using inductively coupled

197   plasma optical emission spectroscopy (ICP-OES).

198

199   **2.4 Thermodynamic modeling**

200   The measured elemental concentration of extracted pore solution was used to calculate

201   the saturation indexes for the anhydrous clinker and hydrate phases. The calculations

202   were performed using the geochemical modeling program GEMS version 3.6.0 [20].

203   Thermodynamic data from the default PSI-GEMS database [21] and the cement-specific

204   data from the CEMDATA18 database [22] were used. The C-S-H was simulated as an

205   ideal solid solution between Jennite, Tobermorite, NaSH, and KSH, based on the CSHQ

206   model originally proposed by Kulik [23]. The carbonate concentrations were estimated

207   assuming saturation with respect to calcite. In addition, undersaturation with respect to

208   C_3S is calculated, using the experimental solubility product of C_3S as suggested by

209   *Nicoleau et al.* [24] and detailed in *Schöler et al.* [25] . Saturation index (SI) is an index

210   that determines the equilibrium condition of a phase with the pore solution. In other

211   words, it indicates whether the pore solution is saturated, undersaturated, or

212   supersaturated with respect to a particular phase. SI is calculated as given in Eq. (3).

$$SI = \log_{10}\left(\frac{IAP}{K_{sp}}\right) \tag{3}$$

213   Where *IAP* is the ion activity product calculated from the measured concentration (from

214   ICP-OES), and K_{sp} is the (theoretical) solubility of the phase in question.

215

216   **3. Results and discussions**

217   **3.1 Calorimetry**

218   **3.1.1 Preliminary dosage study**

219   A summary of the isothermal calorimetry results of cement paste produced with increasing

220   dosages of CO_2 is shown in Fig. 2. The most pronounced effect on hydration (primarily in

221   terms of an increase in the total heat release) was obtained at 0.5% of CO_2 where there was

222   a 23% increase in the total heat at 48 hours. Detailed quantitative analyses of the

223   calorimetry are included in Section 3 of the Supplementary Information. A dose at 0.3%

224   CO_2 had a similar response as the 0.5% dose; it is within the typical dosage range (0.1 -

225   0.3%) of the industrial use of the technology and was selected as the dosage of interest for

226   further investigation.
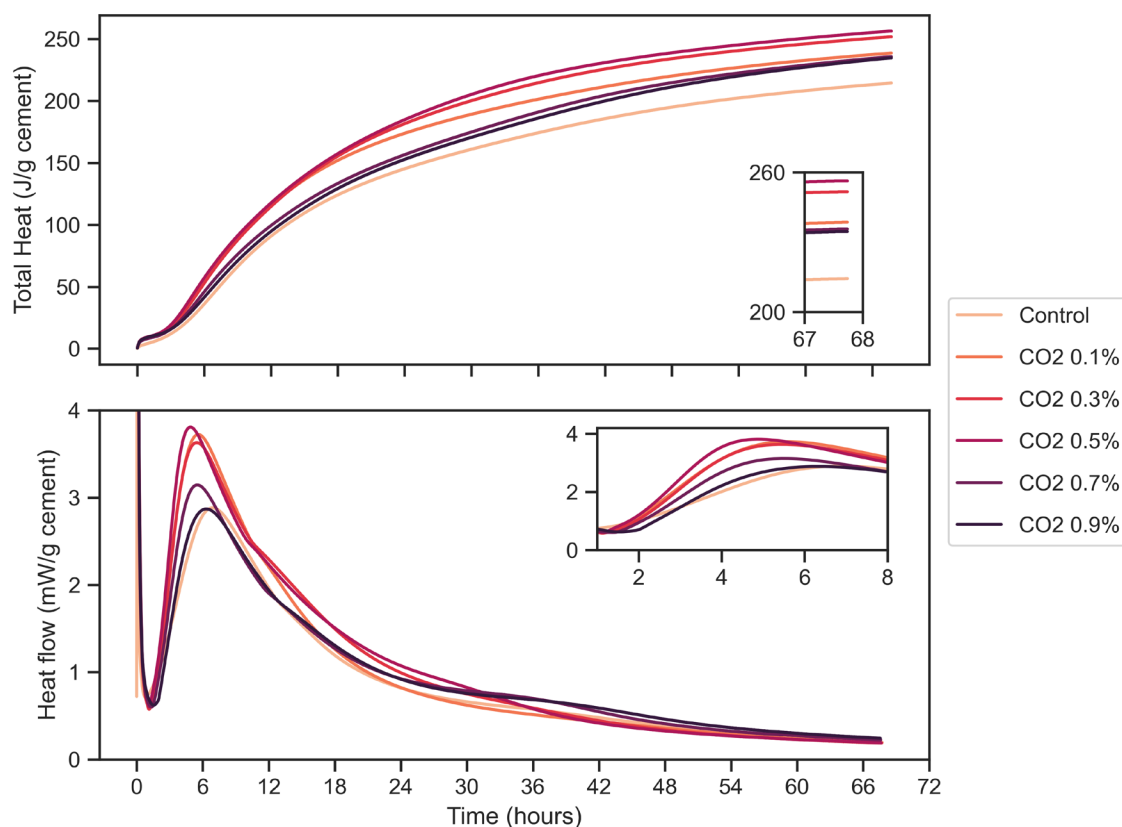
227

Fig. 2. Calorimetry curves of cement dispersions prepared with different percentages of CO_2

230

3.1.2   Comparison of two binder systems

232   The isothermal calorimetry results through 48 h of hydration in cement and tricalcium

233   silicate systems (control condition and dosed with 0.3% CO_2 by weight of binder) are

234   presented in Fig. 3 with analytical observations reported in Table 2. The addition of CO_2

235   imparted an acceleration (shift of the power curve to earlier times) in both systems. The

10

ASTM C1679 thermal indicator of setting time [26] was calculated to be 11.6 h in the control tricalcium silicate system. The CO_2 imparted a 4.7 h decrease to 6.9 h. The time at peak power decreased from 20.5 h in control to 10.6 h in the CO_2 sample. The heat flow at the peak increased by 18% due to CO_2 addition. In the cement system, the control set time by calorimetry was 4.5 h, reducing to 4.1 h under influence of CO_2. The CO_2 addition changed the time at peak power from 6.9 to 5.4 h and increased the corresponding heat flow by 26%.
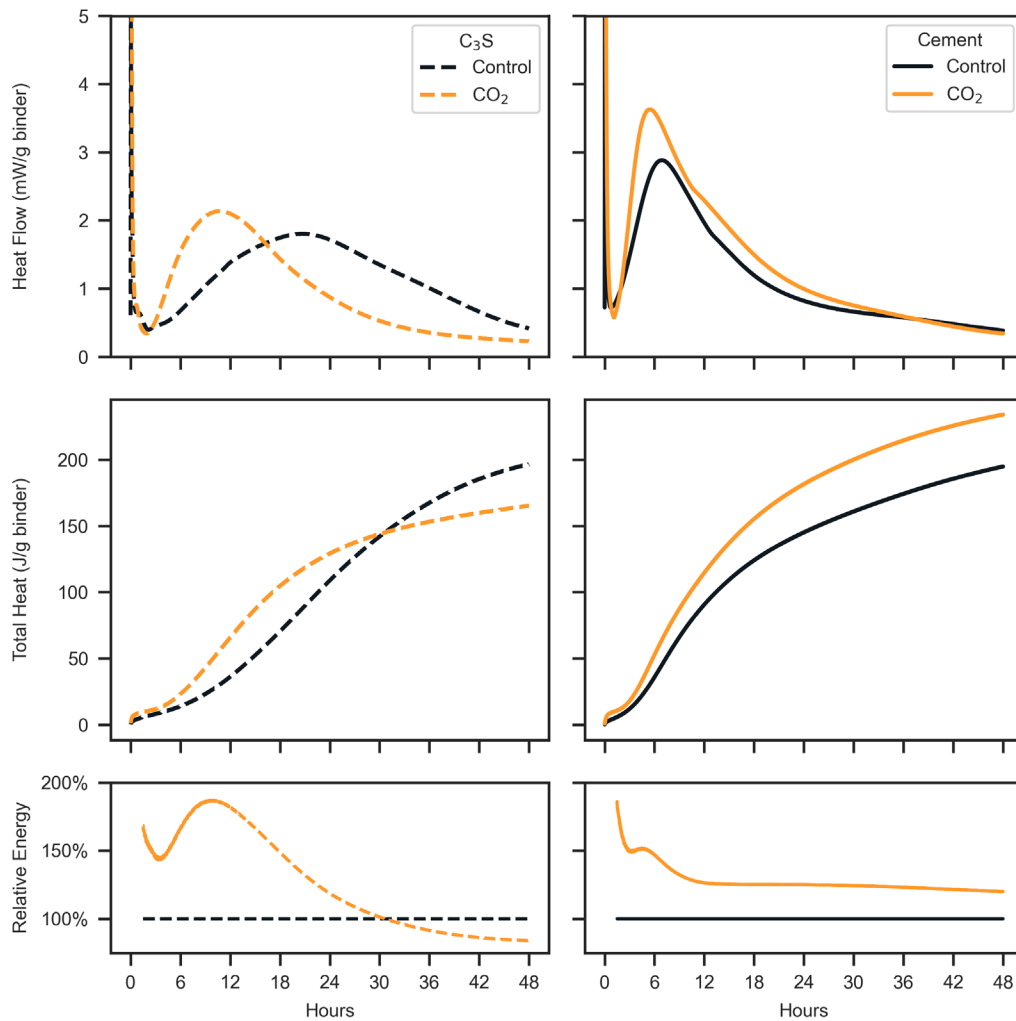
Fig. 3. Isothermal calorimetry (power and energy and energy relative to the control) from cement (left) and tricalcium silicate (right) in the control and 0.3% CO_2 addition conditions

Table 2: Calorimetry curve analysis

Metric	C_3S Reference	C_3S CO_2	Cement Reference	Cement CO_2
Thermal indicator of set (h)	11.6	6.9	4.5	4.1
Acceleration slope ($mW \cdot g^{-1} \cdot h^{-1}$)	0.11	0.20	0.48	0.70
Time at peak heat flow (h)	20.5	10.6	6.9	5.4
Heat flow at peak (mW/g_{cement})	1.80	2.13	2.88	3.63
Total heat at 24 hours (J/g_{cement})	109	129	145	182
Relative total heat at 24 hours	100%	119%	100%	125%
Total heat at 48 hours (J/g_{cement})	197	165	195	234
Relative total heat at 48 hours	100%	84%	100%	120%

An increased heat of hydration (upward shift of energy curve) was observed across the
observation period in the C_3S system through the first 24 h (19% increase) before
becoming equivalent to the control at around 30 h and 16% less at 48 h. In the cement
system, the CO_2 increased the energy at all times of observation with an increase of 25%
at 24 h and 20% at 48 h.

3.2 pH changes

The changes in pH of the pore solutions extracted from C_3S and cement systems with and
without CO_2 are shown in Fig. 4. The pH of control C_3S samples varied over a narrow
range (between 12.64 and 12.74), while the pH of samples with injected CO_2 was slightly
lower at the initial stages (initial observation of 12.40 at 1 min and 12.48 at 6 min),
before becoming comparable to the control samples at 60 min and beyond. The cement
system exhibited a similar pH response. The pH of control samples was around 12.80
throughout the test period of 180 min of hydration. The samples with injected CO_2
showed a slight reduction in the pH at the start of hydration (12.26) that was maintained
through 6 min (pH = 12.28), which was the first common time of comparison to the

268   control system (pH = 12.79). The pH in the CO_2 system increased monotonically during

269   the first 30 min of hydration to settle at values comparable to that of control samples. In

270   both case the CO_2 addition acidified the pore solution temporarily with a full recovery
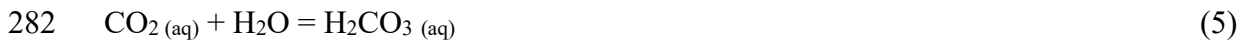
271   within 60 min.

272
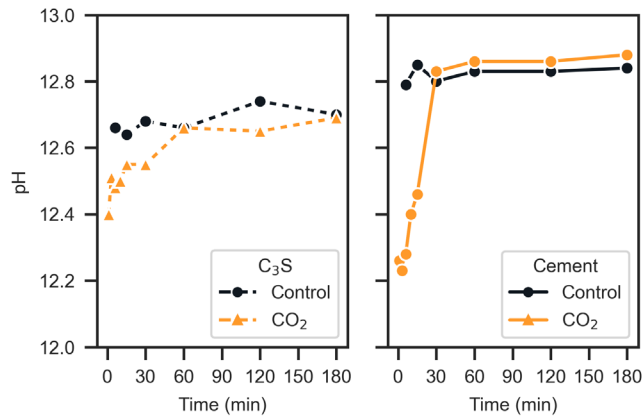
273

274   **Fig. 4. Evolution of pore solution pH in C_3S and cement pastes in the absence or**
275   **inclusion of an addition at 0.3% CO_2 by weight of the binder during the sample**
276   **mixing**

277

278   It is suggested that the action of the CO_2 led to a rapid decrease of pH of the solution at

279   initial times of hydration through a multi-step dissociation reaction:

280

281    $CO_2{}_{(g)} = CO_2{}_{(aq)}$ (4)

282    $CO_2{}_{(aq)} + H_2O = H_2CO_3{}_{(aq)}$ (5)

283    $H_2CO_3{}_{(aq)} = HCO_3^-{}_{(aq)} + H^+$ (6)

284    $HCO_3^-{}_{(aq)} \leftrightarrow CO_3^{2-}{}_{(aq)} + H^+$ (7)

285

286   Over the subsequent 30 to 60 min, the pH increased though the reaction of $Ca(OH)_2$ and

287   precipitation of $CaCO_3$ and the production of OH- to neutralize the acid.

288

289    $Ca(OH)_2 + CO_3^{2-} = CaCO_3 + 2OH^-$ (8)

290

13

291 It was observed that CO_2 caused a greater decrease in the pH of the cement pore solution

292 compared to that of the C_3S pore solution. As presented later (Fig. 7), the reduction in the

293 Ca/Si ratio of cement pore solution upon CO_2 injection was higher than observed in the

294 corresponding C_3S pore solution. C-S-H with a lower Ca/Si ratio generally leads to an

295 increase in alkali uptake by C-S-H, which reduces the pH of the pore solution [27–29]. A

296 high initial concentration (50-75 mmol/L) of sulfur (present as SO_3^{2-}) in cement pore

297 solution (Fig. 6) would also have lowered the dissolved hydroxide concentration, thereby

298 lowering the pH significantly as the electroneutrality of the solution had to be maintained

299 [27].

300

301 **3.3 Pore solution chemistry**

302 The elemental molar concentrations (measured by ICP-OES) present in C_3S and cement

303 pore solutions are presented in Fig. 5 and Fig. 6, respectively. Additional analysis is

304 presented in Section 4 of the Supplementary Information. The precision of the

305 equipment/technique was described as 1-2%. Differences are identified where the

306 compared results are more than 5% different thereby being conservatively outside of the

307 expected reproducibility of the measurements. Effects (increases or decreases) observed

308 in the CO_2 activated systems at the earliest times of common observation (6 min) but

309 diminishing at subsequent ages are understood as valid observations according to

310 alignment with trends established at 1, 3 and 10 min observations that were not made in

311 the control systems.

312

313 Pore solutions of C_3S samples contained a high concentration of Ca (around 20 mmol/L),

314 followed by those of the alkalis (Na and K). The concentrations of other elements (Si, Al,

315 Mg, and Fe) were less than 0.1 mmol/L for the entire tested duration. Differences

316 observed between the control and the CO_2 cases were evident in the Ca and alkalis. At

317 the first observation of CO_2 system, the Ca concentration was about half that of the

318 average reference concentration across the analytical period. At times of common

319 observations, the Ca was reduced 24% at 6 min before recovering to 13% less at 60 min

320 and within 7% at 180 min. The concentration of Si was elevated an average of 6% across

321 the observation period. The other elements were present in trace quantities in the starting

322 material. The concentration of Al was an average 20% lower through the first 60 min and

323 comparable thereafter. The alkalis, Na and K, was 15% and 8% lower in the CO_2

324 activated solution across the observation period. The Mg concentration increased 16% at

325 6 min, remained 10% greater through 60 min and was comparable thereafter. The S

326 concentration increased 25% at 6 and 10 min, was 10% greater through 120 min, and

327 comparable thereafter. The Fe concentration was not changed by the CO_2 activation.
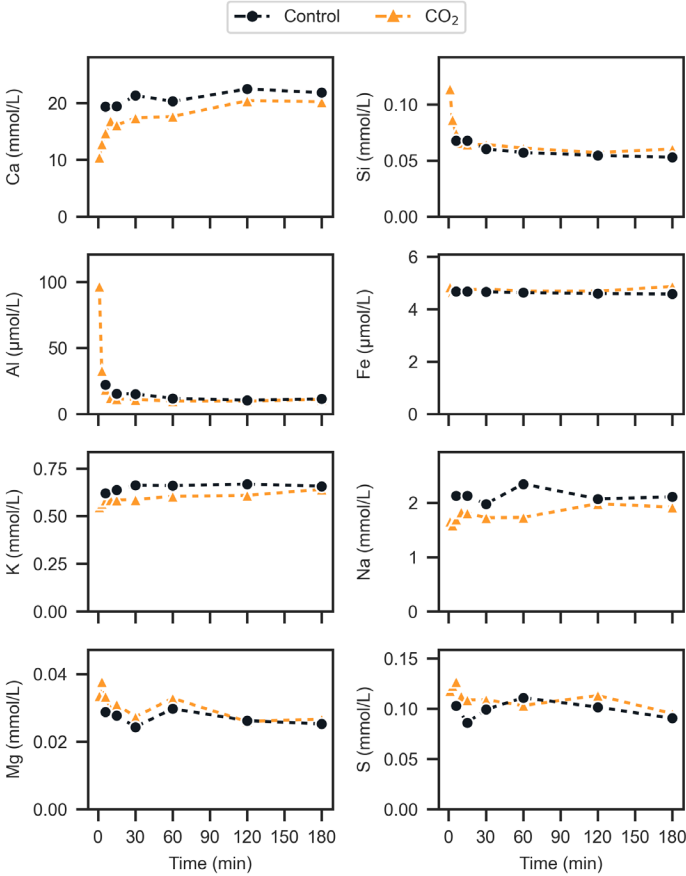
328

Fig. 5. Measured molar concentrations present in pore solution of C$_3$S pastes in the absence or inclusion of an addition at 0.3% CO$_2$ by weight of the binder during the sample mixing
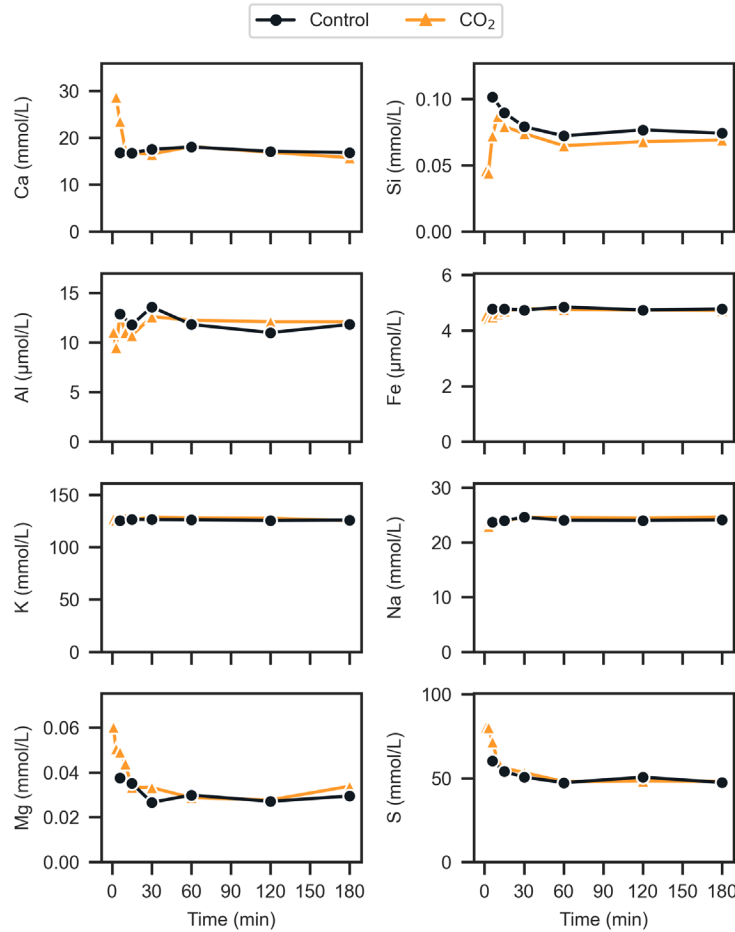
Fig. 6. Measured molar concentrations present in pore solution of cement pastes in the absence or inclusion of an addition at 0.3% CO_2 by weight of the binder during the sample mixing

The level of the Ca concentration in the cement pore solution was slightly lower than that in the C_3S pore solution (around 17 mmol/L). At the first observation of CO_2 system, the Ca concentration was about 60% greater than what the average reference concentration was across the analytical period. At times of common observations, the Ca was increased 40% at 6 min and comparable to the control thereafter. The concentration of Si was lower across the observation period with a reduction of 29% at 6 min and 7 - 12% at later times. Al, Fe, Na and K were not changed significantly by the CO_2. The Mg concentration was about double what the average reference concentration was across the analytical period at the first observation, about 30% greater at 6 min, and close to the control thereafter. The S concentration was 19% greater than the control at 6 min and comparable thereafter.

16

347

348 The ratios of Ca/Si in solution with time for the two binder systems are shown in Fig. 7.

349 The Ca/Si in the solution phase can influence Ca/Si within, and thus the mechanical

350 properties of, C-S-H gel that would be forming [30,31]. The activated C_3S showed a

351 much lower ratio initially compared to later ages, whereas in the activated cement the

352 initial ratio was much higher than it was at later ages. Within the common time

353 comparisons, the Ca/Si of solution at 6 min for the CO_2 activated C_3S was 31% lower

354 than in the control. The ratio increased over time, as it did in the control, but it remained

355 on average 17% lower than the control across the remainder of the observation period.

356 The Ca/Si ratio of the solution phase in the CO_2-activated cement paste was 97% higher

357 than in the control at 6 min and reduced to 13% higher at 15 min. It was thereafter

358 equivalent to, or slightly greater than, the control through to 180 min. The impact in the

359 cement system appeared to be temporary with the Ca/Si development of both systems

360 matching at 10 min and beyond. As supported by the data in Fig. 8, the initial response in

361 the C_3S is for the CO_2 to decrease the Ca in solution and increase the Si, whereas in

362 cement, it acted to increase the Ca and decrease the Si.
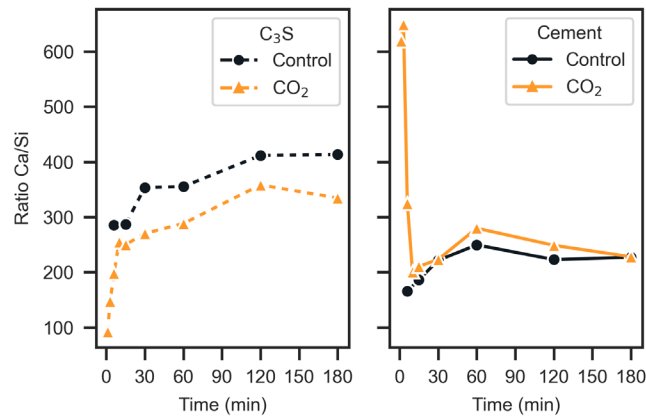
363

364 **Fig. 7. Evolution of Ca to Si ratio in pore solution of C_3S and cement pastes in the**
365 **absence or inclusion of an addition at 0.3% CO_2 by weight of the binder during the**
366 **sample mixing**
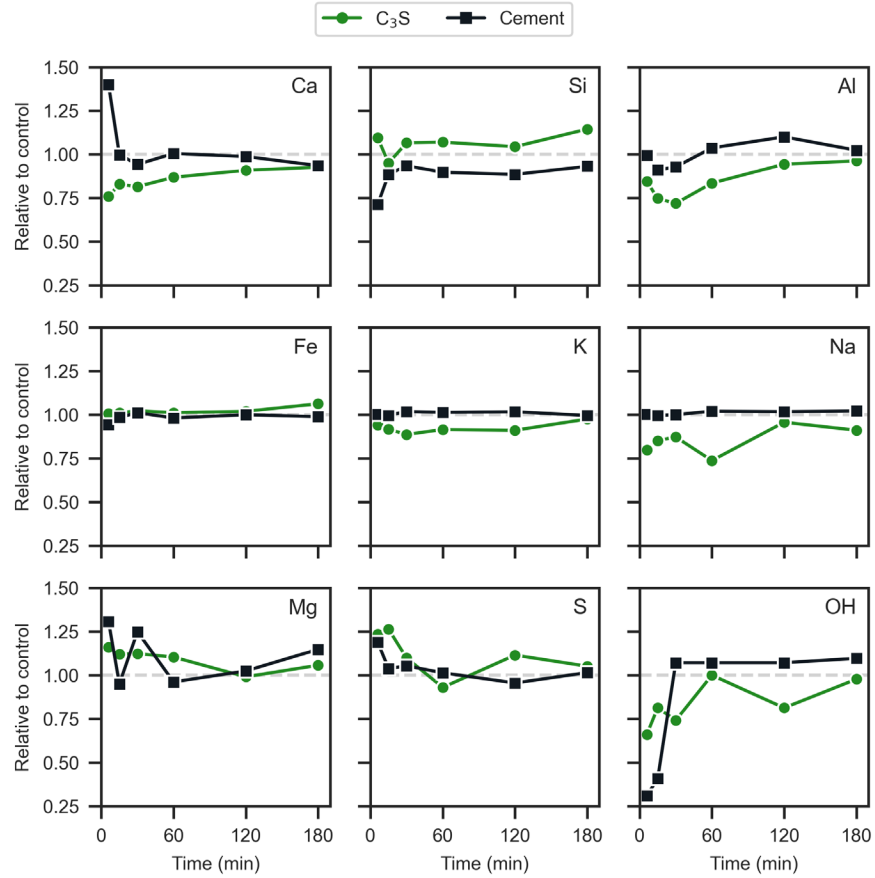
Fig. 8. Molar concentrations in pore solution relative to the control at common times of comparison for C₃S and cement pastes including an addition at 0.3% CO₂ by weight of the binder during the sample mixing
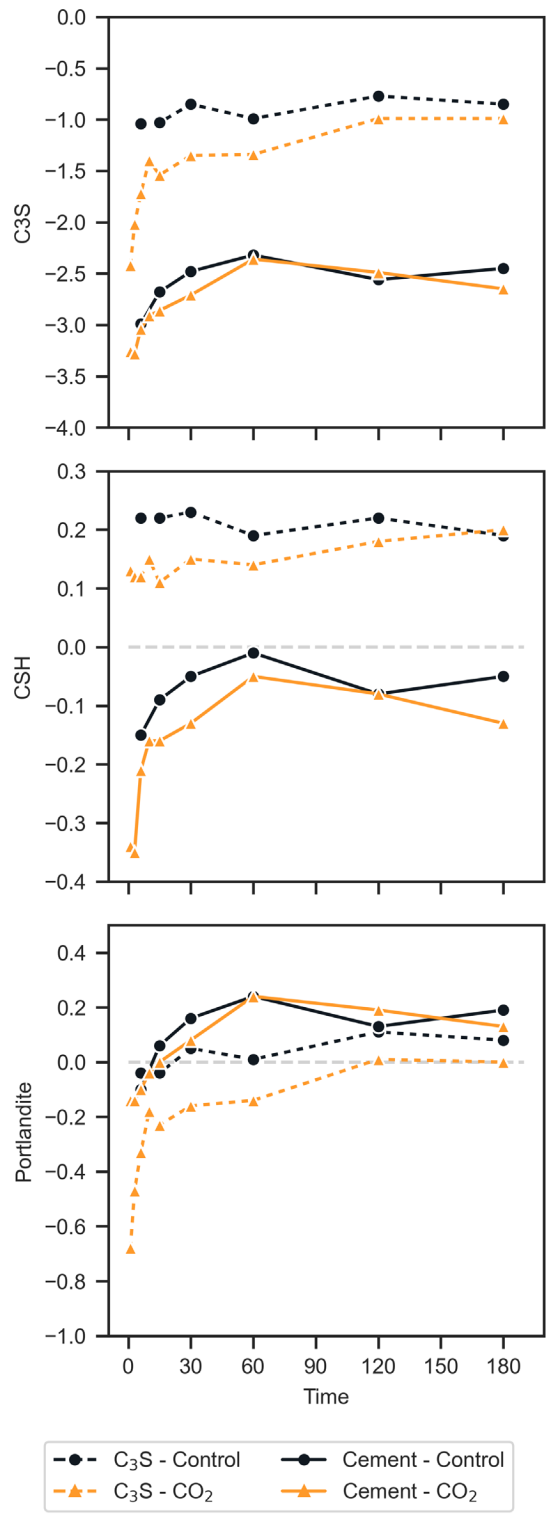
3.4 Saturation indices

Cement hydration is a dissolution-precipitation process wherein the anhydrous material dissolves in the solution, and the hydrates precipitate from the solution [32]. Saturation index (SI), calculated as per Eq. (3), provides the possibility of the two processes occurring vis-à-vis an anhydrous or hydrate phase. SI can either be positive, negative, or zero (equilibrium). A positive value implies oversaturation, suggesting the probability of the precipitation of a phase, while a negative SI implies undersaturation, meaning thereby that the phase is not in equilibrium with the pore solution and is likely to dissolve.

381   Fig. 9 shows the calculated SIs corresponding to the main phases of concern (C_3S, C-S-H

382   gel, portlandite) in the C_3S and cement systems. Concerning the main hydrate phase C-S-

383   H, the reference C_3S system was supersaturated right from the start of hydration (SI = 0 -

384   0.2), while the cement system remained mostly undersaturated (SI = -0.3 to 0). On the

385   other hand, both reference systems were undersaturated (in general) with respect to

386   portlandite for the first 30 min of hydration, suggesting a lesser chance of its

387   precipitation, after which SIs became positive, supporting likely precipitation. The

388   saturations with respect to C-S-H and portlandite were affected similarly upon CO_2

389   injection. In sync with earlier observed effects of CO_2 on chemistry and pH of pore

390   solution (sections 3.2 and 3.3), the over/under-saturation (w.r.t C-S-H and portlandite) of

391   the CO_2-injected system was lower than that of control during the first 30 min of

392   hydration but the differences were reduced at later times. This observed effect can be

393   attributable to the initial pH values in the presence of CO_2.

394

395

Fig. 9. Saturation indices of C₃S, CSH, and Portlandite

397

398

399 The addition of CO_2 in both cases (C_3S and cement) increased the undersaturation with

400 respect to C_3S; the impact was stronger in the case of C_3S paste, where the calcium

401 concentrations were clearly decreased in the presence of CO_2. This stronger

402 undersaturation persisted up to 3 h (and possibly longer), which could explain the faster

403 reaction of C_3S in the presence of CO_2 observed by isothermal calorimetry (see Fig. 3).

404 The undersaturation with respect to C_3S is much stronger in the case of the cement as

405 compared to the C_3S binder.

406

407 The dissolution of C_3S and the corresponding precipitation of C-S-H and portlandite are

408 linked in series. If either of the two processes is near equilibrium, the other controls the

409 hydration kinetics [33]. SI values of the two hydrates (Fig. 9; close to zero) indicated

410 them to be near-equilibrium conditions, implying that the constraints pertaining to C_3S

411 dissolution were more critical than those corresponding to hydrate precipitation, which

412 could be related to the relatively high sulfate concentrations of 50 mM and more

413 observed in the presence of PC. *Nicoleau et al*. [34] concluded that sulfate (in addition to

414 Al) has an inhibiting effect on C_3S dissolution. Therefore, it can be postulated that the

415 high sulfate concentrations limits C_3S dissolution in the PC system. Overall, the

416 calculated SIs and the underlying mechanisms elucidated that the effect of CO_2 on the

417 precipitation of main hydrate phases was limited to the initial stages of hydration.

418

419 For the entire tested duration, both the systems remained supersaturated with respect to

420 ettringite, monosulfate and hydrotalcite; however, the supersaturation was much lower

421 for the C_3S system. The reason being that those phases require sulfate and Mg,

422 respectively, to precipitate, and since those are trace elements in tricalcium silicate, their

423 elemental concentrations in C_3S as compared to cement pore solution were very low, as

424 also observed experimentally (Fig. 5). No significant effect of CO_2 injection on the

425 saturation indices regarding those phases was observed.

426

3.5 TGA

The mass loss TGA curves of all samples are included in Section 5 of the Supplementary Information. For purposes of the present analysis, mass losses in the ranges of 105 - 350 °C (taken as loss of bound water from C-S-H gel), 350 - 550 °C (the dehydroxylation of portlandite), and 550°C - 1000 °C (the decomposition of carbonates) were quantified. Further quantitative analysis of the weight losses was made with the derivative of the weight loss plot (derivative thermal gravimetry or DTG) to better characterize the carbonate mass loss in terms of amorphous and crystalline carbonates.

Only times of common comparison between the two conditions are included in the analysis. A summary of the evolution with hydration time of the total mass loss and specific mass losses (carbonates, total bound water, bound water in C-S-H gel and bound water in calcium hydroxide) for both the C_3S and cement systems, including the anhydrous condition, is shown in Fig. 10. The mass losses for each binder were normalized to the final mass (after heating to 1000 °C) of the anhydrous binder to allow all mass losses to be expressed on the same basis as the dosage of the CO_2, i.e., as percentages by weight of the anhydrous binder.
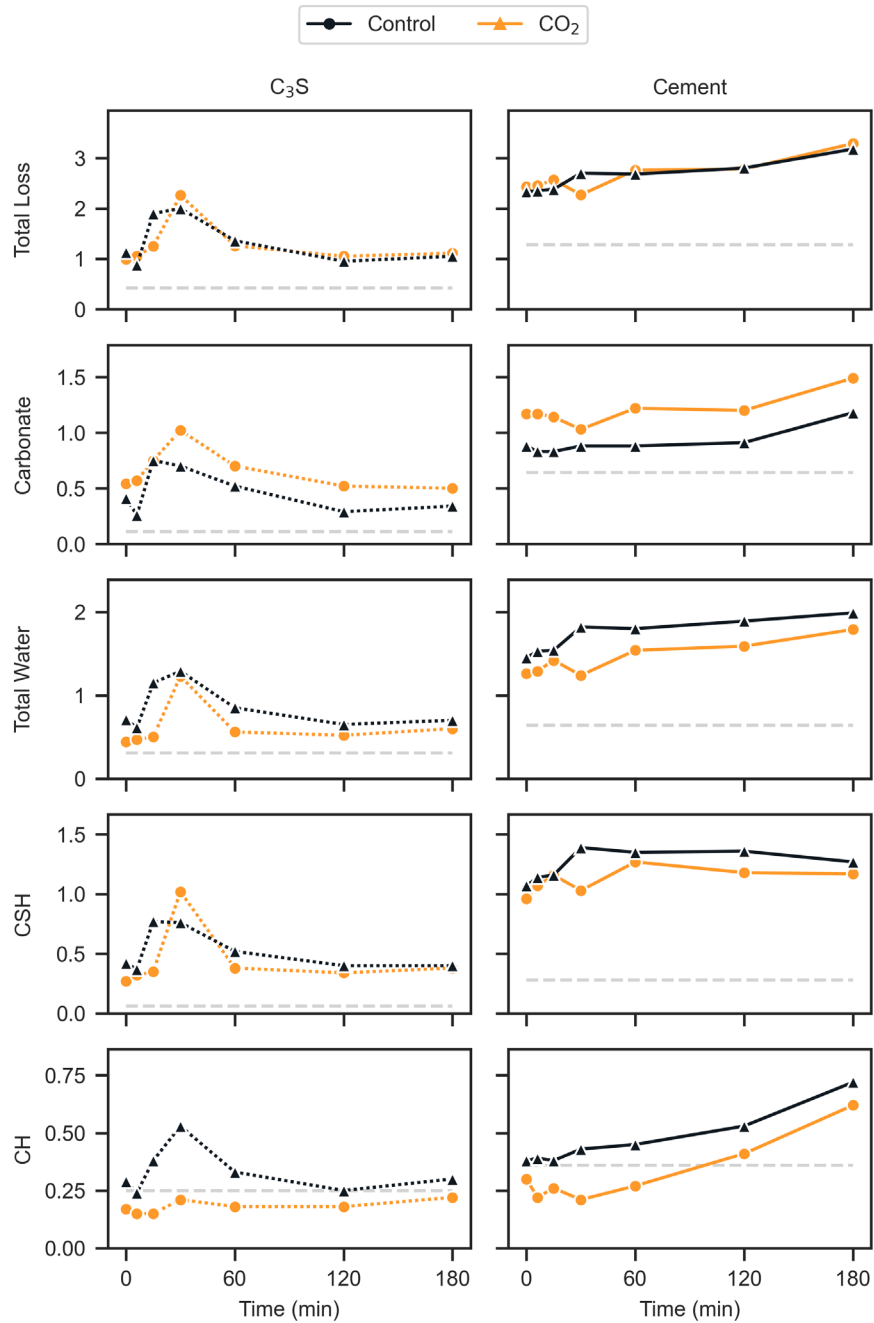
Fig. 10. Weight losses (by % of original cement) as measured by TGA. Reported as the total loss, loss associated with carbonates, total loss associated with bound water, loss of bound water from C-S-H gel, and loss of bound water from portlandite

The anhydrous C_3S had a total mass loss of 0.42%. The total mass was greater (about 1%) than the initial state in both conditions (reference or CO_2) but it did not show an

452 increasing trend with hydration time. An increased total mass loss observation in both

453 conditions at 15 and 30 was likely an aberrant result since the solution phase analysis and

454 thermodynamic modelling did not identify any temporally synchronous anomalies. The

455 total mass loss on the cement increased with time. The anhydrous cement had a total

456 mass loss of 1.28% whereas for the initial states of the analyzed samples it was around

457 2.4% and then increased to around 3.4% by the end of the observation period. The total

458 mass loss includes loss of water from C-S-H, water from calcium hydroxide, and CO_2

459 from carbonates. The CO_2 systems had lower amounts of calcium hydroxide and CSH,

460 and greater amounts of carbonate. The average amount of calcium hydroxide formed in

461 the CO_2 activated C_3S was about 40% less across the observation period although the gap

462 closed to 30% less in the final two observations. Likewise, the cement averaged about

463 30% less calcium hydroxide than in the reference but was within 20% at three hours

464 hydration. The gel mass loss was about 15% less than the reference in the C_3S system and

465 10% less in the cement system

466

467 Quantitatively, the C_3S samples activated with CO_2 showed an average total net

468 carbonate gain of 0.21% (excluding comparisons to the anomalously elevated carbonate

469 content in the control at 15 and 30 min). The cement system with injected CO_2 showed an

470 average 0.27 wt.% higher carbonate weight loss than the corresponding control sample.

471 The net carbonate increase in the cement system is very close to the amount of CO_2 dosed

472 to the system (0.3% by weight of cement). The data from the cement system implied a

473 90% mineralization efficiency, while in the C_3S system, it was closer to 75%.

474

475 Analysis of the DTG mass loss peak attributable to the carbonate (data considered over

476 the span 450°C to 750 °C) allowed a deconvolution of the overlapping peaks of

477 amorphous carbonate and crystalline carbonate (examples and results summary provided

478 in Section 6 of the Supplementary Information). Amorphous carbonate was identified

479 (with an average observed onset of 550 °C and peak at 605 °C) as a mass loss

480 abutting/adjacent to the main carbonate mass loss (average peak of 650 °C). The

481 conclusion is consistent with the work of *Thiery et. al.* [35] who identified amorphous

482 carbonate decomposition starting at 550 °C and crystalline carbonate decomposition at

483 higher temperatures. The two carbonate forms suggest differing degrees of crystallinity

484 and modes of formation [36,37].

485

486 Increases to the carbonate content of the hydrated system were only of amorphous

487 carbonate (an average net 0.12% if excluding the anomalously high carbonate data at 15

488 and 30 min). It is likely that the carbonates in these cases were attributable to

489 environmental exposure. The addition of the CO_2 in the C_3S system resulted in an greater

490 total carbonate content (average 0.21% mass loss) that was representative of crystalline

491 calcium carbonate.

492

493 The anhydrous cement sample contained a small amount CO_2 bound in amorphous

494 carbonate (0.08% mass loss) and a larger amount of bound CO_2 within crystalline

495 carbonate (0.58%). The crystalline carbonate would have come from the raw materials

496 for the cement. The addition of the CO_2 to the cement system caused a net increase in

497 total carbonate of 0.27% of which 48% was amorphous.

498

499 **3.6 SEM**

500 The hydration product formation in the hydrating C_3S and cement systems was evaluated

501 through SEM. As a baseline condition, the micrographs of as-received anhydrous C_3S

502 and cement were captured (see Section 8 of the Supplementary Information). The

503 surfaces of anhydrous particles can be observed to be bare, with some flecks of

504 irregularly shaped debris. An unreacted surface was understood as the baseline condition

505 for subsequent further analysis of hydrated systems.

506

507 Fig. 11 presents the micrographs of C_3S paste (control and CO_2) at different hydration

508 times. The surfaces of all hydrated C_3S samples were covered with hydration products (as

509 assessed in comparison to view of the anhydrous starting condition). Rhombohedral-

510 shaped formations with a characteristic dimension of 0.4 - 0.7 μm were present on the

511 surfaces of CO_2-activated samples right from the first observation (one minute after the

512 end of the mixing under the CO_2 injection) up until 60 min. The rhombohedral shape is

513 typical of a crystalline calcite form of calcium carbonate [38–41], which pointed towards

514   the development of calcite through the mineralization of CO_2. This was confirmed by

515   performing EDS on a rhombohedral site of interest identified in the CO_2-activated C_3S

516   sample hydrated for 3 min (see Section 8 of the Supplemental Information). The EDS

517   spectrum (Fig. 12) showed the presence of Ca, O, and C. While detection of carbon is

518   very common for EDS since even the smallest contamination with organic materials can

519   show the presence of C (e.g., from conductive carbon glue tape used to place the sample),

520   the morphology and absence of a signal from Si indicated that the rhombohedral

521   formations were not a silicate but rather a carbonate particle.

522
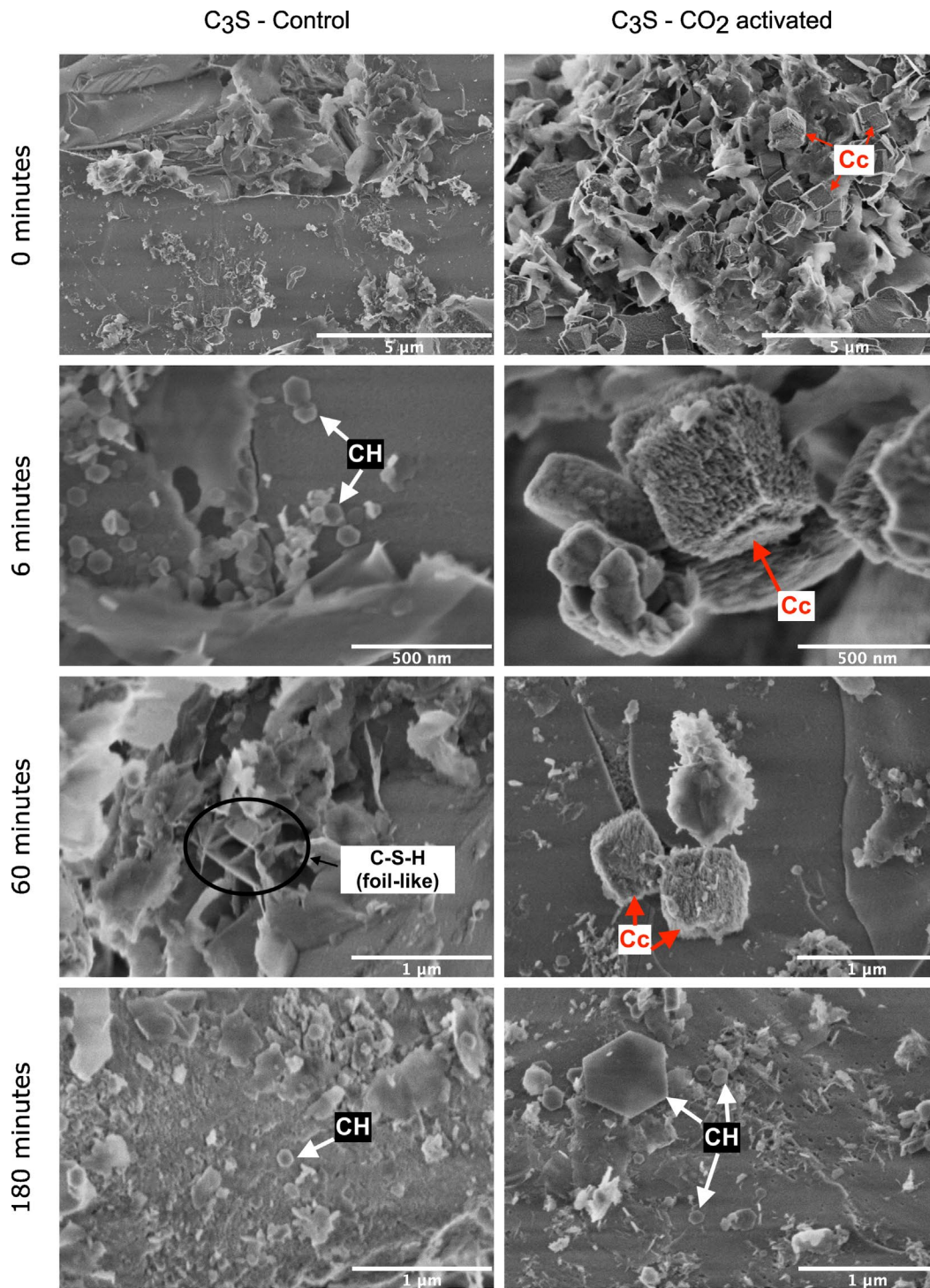
Fig. 11. SEM micrographs showing the formation of hydration products (with time) in C₃S, control and CO₂ activated paste (Cc: Calcium carbonate; CH: Portlandite)

527
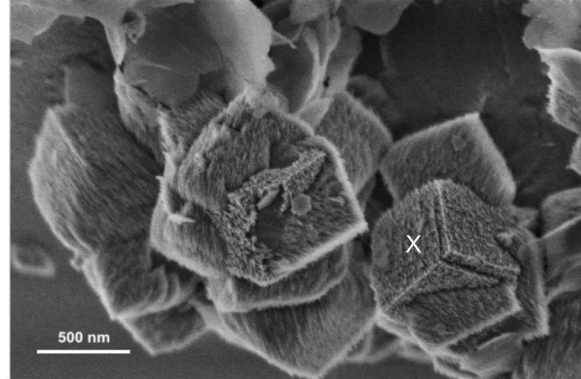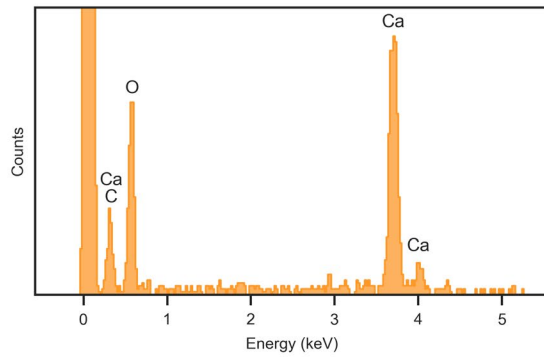
528

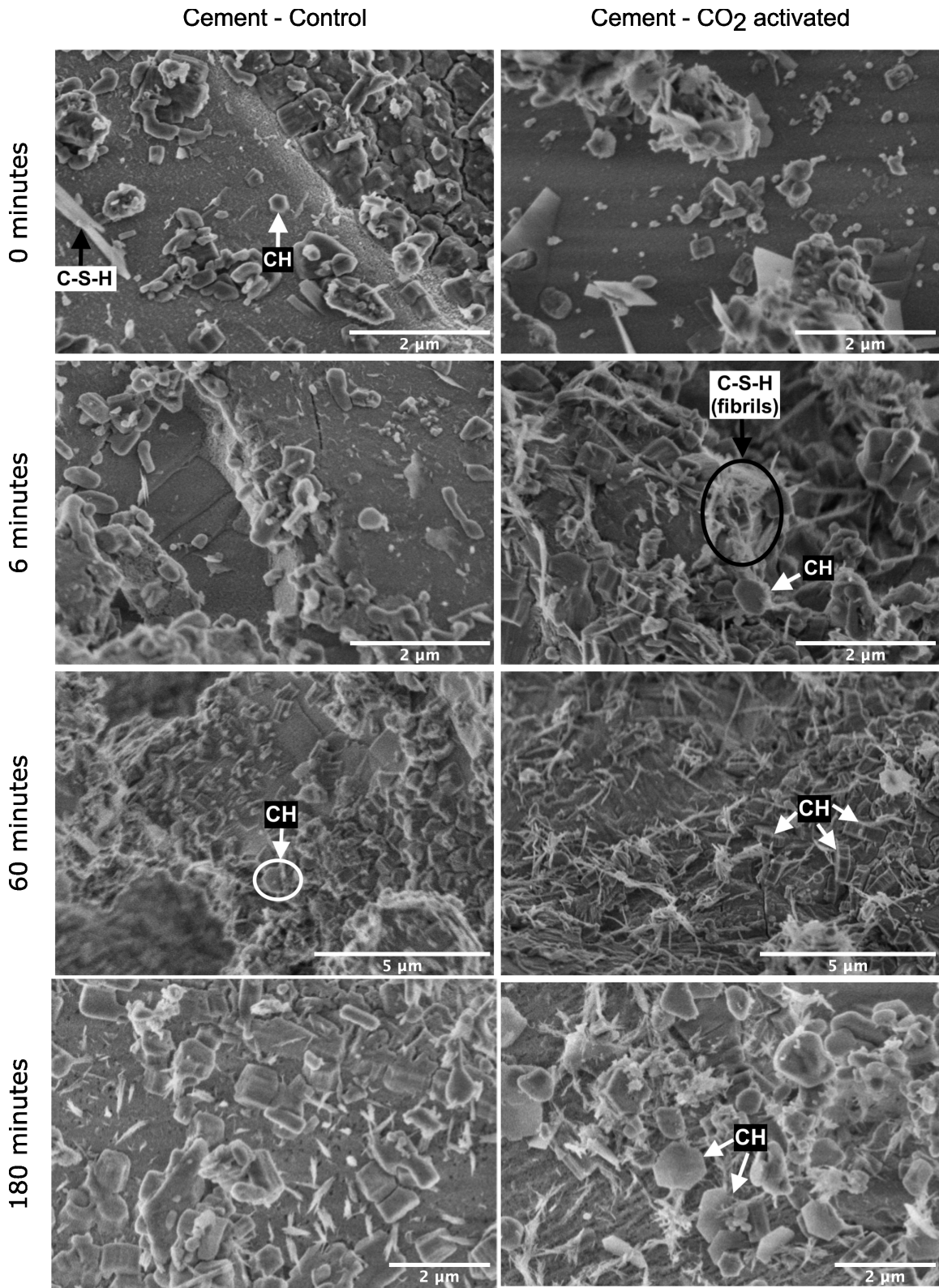**Fig. 12. EDS spectrum (left) of rhombohedral products observed in C₃S sample activated with CO₂ at 3 min (right). Analyzed particle indicated with an ×**

531

The micrographs of cement paste (control and CO_2-activated) at different hydration times are shown in Fig. 13. There is a notable abundance of hydration products in all cement samples starting from time zero (the conclusion of 90 s of mixing) through to 180 min of hydration. Samples at 0 min (both control and with injected CO_2) show the development of C-S-H. A few hexagonal crystals of $Ca(OH)_2$, approximately 100 to 300 nm in size, can also be spotted.

Cement - Control

Cement - CO₂ activated

0 minutes

6 minutes

60 minutes

180 minutes

C-S-H

CH

C-S-H (fibrils)

CH

CH

CH

CH

2 µm

5 µm

Fig. 13. SEM micrographs showing the formation of hydration products (with time) in cement, control and CO₂ activated paste (Cc: Calcium carbonate; CH: Portlandite)

538

539
540
541

542

543 In the case of cement samples with injected CO_2, calcium carbonate crystals were not

544 clearly observed, despite a considerable increase of carbonate content according to TGA.

545 This can be due to either covering of carbonate crystals by other hydration products or a

546 possible formation of amorphous $CaCO_3$ or a difficulty associated with increased

547 heterogeneity of the cement with respect to the C_3S.

548

549 ## 4. Conclusions

550 The early-age changes (up to 3 h) occurring in the C_3S and cement systems activated with

551 0.3% CO_2 by mass of binder were analyzed through multiple characterization techniques

552 such as calorimetry, ICP-OES, TGA, XRD, and SEM. The observations add to the

553 knowledge base of using CO_2 as a concrete admixture and improves understanding of the

554 associated performance benefits in ready mixed concrete production. Specific

555 conclusions from this study are as follows:

556 • CO_2 activation caused an acceleration of hydration of C_3S and cement as

557   demonstrated through decreased time to thermal set, increased slope of the main

558   hydration peak, and increased maximum energy release at the hydration peak. In

559   cement, the CO_2 led to greater energy release across the 48 h observation period, with

560   a 20% increase over the control at the conclusion. In C_3S, the total energy release was

561   19% more than the control at 24 h, equivalent at 30 h, and 16% lower at 48 h.

562 • Consumption of $Ca(OH)_2$ in the CO_2 mineralization process reduced the pH of both

563   the binder systems during the first 30 to 60 min of hydration. However, at later times

564   it had rebounded to the level of control sample pH.

565 • CO_2 mineralization also affected the elemental concentrations observed in the C_3S

566   and cement pore solutions. Compared to control, the CO_2-activated C_3S solution

567   showed slightly but consistently lower concentrations of calcium and alkalis (Na and

568   K). On the other hand, the CO_2-activated cement solution contained higher

569   concentrations of calcium and sulfur (compared to control) only during the first few

570   min of hydration. No significant change in the alkali concentration was observed.

571 • The Ca/Si ratio of the C_3S and cement pore solutions were impacted differently upon

572   CO_2 activation. Compared to their control counterparts, CO_2 led to lower ratios in the

573   C_3S system, while the ratios were higher in the cement system during the first 10 min

574   of hydration. Thereafter, ratios equivalent to control were maintained in the cement

575   system, while it remained lower than the control in the C_3S system.

576   •   The observed formation of calcium carbonate in both the CO_2-activated binder

577   systems indicate a strong driving force for the precipitation of carbonates upon CO_2

578   activation.

579   •   The total amount of reaction products, as detected by TGA in terms of bound water

580   and CO_2, was similar between the two conditions, for both binders, across the first

581   180 min of hydration. The CO_2-activated systems had an increase in the amount of

582   carbonate and a corresponding decrease in the amount of C-S-H and CH formed.

583   •   SEM micrographs exhibited a multitude of rhombohedral-shaped calcite (confirmed

584   through EDS) crystals in the CO_2-activated C_3S system up until one hour of

585   hydration, while only a few such crystals were spotted in the cement system.

CRediT authorship contribution statement

Sean Monkman: Conceptualization, Methodology, Formal analysis, Writing - review and editing, Funding acquisition.

Yogiraj Sargam: Formal analysis, Writing - original draft, Writing - review and editing.

Olga Naboka: Methodology, Investigation, Supervision, Initial analysis, Writing - original draft, Writing - review and editing.

Barbara Lothenbach: Formal analysis, Writing - review and editing.

Declaration of Competing Interest

The authors declare that they have no known competing financial interests or personal relationships that could have appeared to influence the work reported in this paper.

Data Availability

Data will be made available on request.

Acknowledgements

References

[1] P.J.M. Monteiro, S.A. Miller, A. Horvath, Towards sustainable concrete, Nature Mater. 16 (2017) 698–699. https://doi.org/10.1038/nmat4930.

[2] S.A. Miller, V.M. John, S.A. Pacca, A. Horvath, Carbon dioxide reduction potential in the global cement industry by 2050, Cement and Concrete Research. 114 (2018) 115–124. https://doi.org/10.1016/j.cemconres.2017.08.026.

[3] IEA, Net Zero by 2050, Fourth revision, IEA Publications, Paris, 2021. https://www.iea.org/reports/net-zero-by-2050.

616 [4] A. Favier, C. De Wolf, K. Scrivener, G. Habert, A sustainable future for the
617   European Cement and Concrete Industry: Technology assessment for full
618   decarbonisation of the industry by 2050, ETH Zurich, 2018.
619   https://doi.org/10.3929/ETHZ-B-000301843.

620 [5] CEMBUREAU, Cementing the European Green Deal, European Cement
621   Association, Brussels, 2020. https://cembureau.eu/library/reports/2050-carbon-
622   neutrality-roadmap/ (accessed August 16, 2021).

623 [6] Portland Cement Association, Roadmap to Carbon Neutrality, 2021.
624   cement.org/sustainability/roadmap-to-carbon-neutrality.

625 [7] Global Cement and Concrete Association, Concrete Future - The GCCA 2050
626   Cement and Concrete Industry Roadmap for Net Zero Concrete, London, 2021.
627   https://gccassociation.org/concretefuture/.

628 [8] J. Monteiro, S. Roussanaly, CCUS scenarios for the cement industry: Is CO_2
629   utilization feasible?, Journal of CO_2 Utilization. 61 (2022) 102015.
630   https://doi.org/10.1016/j.jcou.2022.102015.

631 [9] H. Xie, H. Yue, J. Zhu, B. Liang, C. Li, Y. Wang, L. Xie, X. Zhou, Scientific and
632   Engineering Progress in CO_2 Mineralization Using Industrial Waste and Natural
633   Minerals, Engineering. 1 (2015) 150–157. https://doi.org/10.15302/J-ENG-2015017.

634 [10]   H. Ostovari, A. Sternberg, A. Bardow, Rock 'n' use of CO_2: carbon footprint of
635   carbon capture and utilization by mineralization, Sustainable Energy Fuels. 4 (2020)
636   4482–4496. https://doi.org/10.1039/D0SE00190B.

637 [11]   V. Sick, Spiers Memorial Lecture: CO_2 utilization: why, why now, and how?,
638   Faraday Discuss. 230 (2021) 9–29. https://doi.org/10.1039/D1FD00029B.

639 [12]   S. Monkman, M. MacDonald, On carbon dioxide utilization as a means to
640   improve the sustainability of ready-mixed concrete, Journal of Cleaner Production.
641   167 (2017) 365–375. https://doi.org/10.1016/j.jclepro.2017.08.194.

642 [13]   R.L. Berger, J.F. Young, K. Leung, Acceleration of Hydration of Calcium
643   Silicates by Carbon-Dioxide Treatment, Nature: Physical Science. 240 (1972) 16–18.
644   https://doi.org/10.1038/physci240016a0.

645 [14]   S. Monkman, B.E.J. Lee, K. Grandfield, M. MacDonald, L. Raki, The impacts of
646   in-situ carbonate seeding on the early hydration of tricalcium silicate, Cement and
647   Concrete Research. 136 (2020) 106179.
648   https://doi.org/10.1016/j.cemconres.2020.106179.

649 [15]   S. Monkman, Y. Sargam, L. Raki, Comparing the effects of in-situ nano-calcite
650   development and ex-situ nano-calcite addition on cement hydration, Construction and
651   Building Materials. 321 (2022) 126369.
652   https://doi.org/10.1016/j.conbuildmat.2022.126369.

653 [16] S. Monkman, P.A. Kenward, G. Dipple, M. MacDonald, M. Raudsepp, Activation
654   of cement hydration with carbon dioxide, Journal of Sustainable Cement-Based
655   Materials. 7 (2018) 160–181. https://doi.org/10.1080/21650373.2018.1443854.

656 [17] S. Monkman, Sustainable Ready Mixed Concrete Production Using Waste CO2:
657   A Case Study, in: SP-330 Proceedings Fourteenth International Conference: Recent
658   Advances in Concrete Technology and Sustainability Issues, American Concrete
659   Institute, Beijing, China, 2018: pp. 163–174.

660 [18] J.I. Bhatty, Hydration versus strength in a portland cement developed from
661   domestic mineral wastes — a comparative study, Thermochimica Acta. 106 (1986)
662   93–103. https://doi.org/10.1016/0040-6031(86)85120-6.

663 [19] M. Wojdyr, Fityk: a general-purpose peak fitting program, J Appl Crystallogr. 43
664   (2010) 1126–1128. https://doi.org/10.1107/S0021889810030499.

665 [20] D.A. Kulik, T. Wagner, S.V. Dmytrieva, G. Kosakowski, F.F. Hingerl, K.V.
666   Chudnenko, U.R. Berner, GEM-Selektor geochemical modeling package: revised
667   algorithm and GEMS3K numerical kernel for coupled simulation codes, Comput
668   Geosci. (2012). https://doi.org/10.1007/s10596-012-9310-6.

669 [21] W. Hummel, U. Berner, E. Curti, F.J. Pearson, T. Thoenen, Nagra/PSI Chemical
670   Thermodynamic Data Base 01/01, Radiochimica Acta. 90 (2002) 805–813.
671   https://doi.org/10.1524/ract.2002.90.9-11_2002.805.

672 [22] B. Lothenbach, D.A. Kulik, T. Matschei, M. Balonis, L. Baquerizo, B. Dilnesa,
673   G.D. Miron, R.J. Myers, Cemdata18: A chemical thermodynamic database for
674   hydrated Portland cements and alkali-activated materials, Cement and Concrete
675   Research. 115 (2019) 472–506. https://doi.org/10.1016/j.cemconres.2018.04.018.

676 [23] D.A. Kulik, Improving the structural consistency of C-S-H solid solution
677   thermodynamic models, Cement and Concrete Research. 41 (2011) 477–495.
678   https://doi.org/10.1016/j.cemconres.2011.01.012.

679 [24] L. Nicoleau, A. Nonat, D. Perrey, The di- and tricalcium silicate dissolutions,
680   Cement and Concrete Research. 47 (2013) 14–30.
681   https://doi.org/10.1016/j.cemconres.2013.01.017.

682 [25] A. Schöler, B. Lothenbach, F. Winnefeld, M.B. Haha, M. Zajac, H.-M. Ludwig,
683   Early hydration of SCM-blended Portland cements: A pore solution and isothermal
684   calorimetry study, Cement and Concrete Research. 93 (2017) 71–82.
685   https://doi.org/10.1016/j.cemconres.2016.11.013.

686 [26] ASTM C1679-17, Standard Practice for Measuring Hydration Kinetics of
687   Hydraulic Cementitious Mixtures Using Isothermal Calorimetry, ASTM
688   International, West Conshohocken, PA, 2017. https://doi.org/10.1520/C1679-17.

689 [27] B. Lothenbach, K. Scrivener, R.D. Hooton, Supplementary cementitious
690 materials, Cement and Concrete Research. 41 (2011) 1244–1256.
691 https://doi.org/10.1016/j.cemconres.2010.12.001.

692 [28] T. Chappex, K.L. Scrivener, The Effect of Aluminum in Solution on the
693 Dissolution of Amorphous Silica and its Relation to Cementitious Systems, J. Am.
694 Ceram. Soc. 96 (2013) 592–597. https://doi.org/10.1111/jace.12098.

695 [29] T.T.H. Bach, E. Chabas, I. Pochard, C. Cau Dit Coumes, J. Haas, F. Frizon, A.
696 Nonat, Retention of alkali ions by hydrated low-pH cements: Mechanism and
697 Na+/K+ selectivity, Cement and Concrete Research. 51 (2013) 14–21.
698 https://doi.org/10.1016/j.cemconres.2013.04.010.

699 [30] A. Nonat, The structure and stoichiometry of C-S-H, Cement and Concrete
700 Research. 34 (2004) 1521–1528. https://doi.org/10.1016/j.cemconres.2004.04.035.

701 [31] W. Kunther, S. Ferreiro, J. Skibsted, Influence of the Ca/Si ratio on the
702 compressive strength of cementitious calcium–silicate–hydrate binders, J. Mater.
703 Chem. A. 5 (2017) 17401–17412. https://doi.org/10.1039/C7TA06104H.

704 [32] M. Zajac, J. Skocek, B. Lothenbach, B.H. Mohsen, Late hydration kinetics:
705 Indications from thermodynamic analysis of pore solution data, Cement and Concrete
706 Research. 129 (2020) 105975. https://doi.org/10.1016/j.cemconres.2020.105975.

707 [33] J.W. Bullard, G.W. Scherer, J.J. Thomas, Time dependent driving forces and the
708 kinetics of tricalcium silicate hydration, Cement and Concrete Research. 74 (2015)
709 26–34. https://doi.org/10.1016/j.cemconres.2015.03.016.

710 [34] L. Nicoleau, E. Schreiner, A. Nonat, Ion-specific effects influencing the
711 dissolution of tricalcium silicate, Cement and Concrete Research. 59 (2014) 118–138.
712 https://doi.org/10.1016/j.cemconres.2014.02.006.

713 [35] M. Thiery, G. Villain, P. Dangla, G. Platret, Investigation of the carbonation front
714 shape on cementitious materials: Effects of the chemical kinetics, Cement and
715 Concrete Research. 37 (2007) 1047–1058.
716 https://doi.org/10.1016/j.cemconres.2007.04.002.

717 [36] N.C. Collier, Transition and Decomposition Temperatures of Cement Phases - A
718 Collection of Thermal Analysis Data, Ceramics - Silikaty. (2016) 338–343.
719 https://doi.org/10.13168/cs.2016.0050.

720 [37] G. Villain, M. Thiery, G. Platret, Measurement methods of carbonation profiles in
721 concrete: Thermogravimetry, chemical analysis and gammadensimetry, Cement and
722 Concrete Research. 37 (2007) 1182–1192.
723 https://doi.org/10.1016/j.cemconres.2007.04.015.

724 [38] H. Cheng, X. Zhang, H. Song, Morphological Investigation of Calcium Carbonate
725 during Ammonification-Carbonization Process of Low Concentration Calcium

726 Solution, Journal of Nanomaterials. 2014 (2014) 1–7.
727 https://doi.org/10.1155/2014/503696.

728 [39] J. Zhu, L. Huang, M. Cui, L. Ma, Heterostructured calcium carbonate nanowires
729 controlled by a cationic polyelectrolyte, CrystEngComm. 17 (2015) 1010–1014.
730 https://doi.org/10.1039/C4CE02002B.

731 [40] A.C.S. Jensen, A. Brif, B. Pokroy, M. Hinge, H. Birkedal, Morphology-
732 preserving transformation of minerals mediated by a temperature-responsive polymer
733 membrane: calcite to hydroxyapatite, CrystEngComm. 18 (2016) 2289–2293.
734 https://doi.org/10.1039/C5CE02245B.

735 [41] Y. Sargam, K. Wang, A. Tsyrenova, F. Liu, S. Jiang, Effects of anionic and
736 nonionic surfactants on the dispersion and stability of nanoSiO2 in aqueous and
737 cement pore solutions, Cement and Concrete Research. 144 (2021) 106417.
738 https://doi.org/10.1016/j.cemconres.2021.106417.

739

740 **Appendix A. Supporting information**

741 Supplementary data associated with this article can be found in the online version at

742 doi:10.1016/j.jcou.2022.102254.

743

744 **List of Figures**

745 **Fig. 1. Experimental design used in this study**
746 Size: Single column
747 Filename: Figure 01 - flow chart.eps
748
749 **Fig. 2. Calorimetry curves of cement dispersions prepared with different percentages**
750 **of CO_2**
751 Size: 1.5 columns
752 Filename: Figure 02 - all dose calorimetry.eps
753
754 **Fig. 3. Isothermal calorimetry (power and energy and energy relative to the control)**
755 **from cement (left) and tricalcium silicate (right) in the control and 0.3% CO_2 addition**
756 **conditions**
757 Size: 1.5 columns
758 Filename: Figure 03 - calorimetry incl Rel - cement and C3S.eps
759
760 **Fig. 4. Evolution of pore solution pH in C_3S and cement pastes in the absence or**
761 **inclusion of an addition at 0.3% CO_2 by weight of the binder during the sample**
762 **mixing**

763   Size: Single column
764   Filename: Figure 04 - pH.eps
765

766   **Fig. 5. Measured molar concentrations present in pore solution of C_3S pastes in the**
767   **absence or inclusion of an addition at 0.3% CO_2 by weight of the binder during the**
768   **sample mixing**
769   Size: Single column
770   Filename: Figure 05 - ICP - C3S.eps
771

772   **Fig. 6. Measured molar concentrations present in pore solution of cement pastes in**
773   **the absence or inclusion of an addition at 0.3% CO_2 by weight of the binder during**
774   **the sample mixing**
775   Size: Single column
776   Filename: Figure 06 - ICP - Cement.eps
777

778   **Fig. 7. Evolution of Ca to Si ratio in pore solution of C_3S and cement pastes in the**
779   **absence or inclusion of an addition at 0.3% CO_2 by weight of the binder during the**
780   **sample mixing**
781   Size: Single column
782   Filename: Figure 07 - Ratio Ca to Si.eps
783

784   **Fig. 8. Molar concentrations in pore solution relative to the control at common times**
785   **of comparison for C_3S and cement pastes including an addition at 0.3% CO_2 by**
786   **weight of the binder during the sample mixing**
787   Size: 1.5 columns
788   Filename: Figure 08 - C3S and Cement Relative to ref.eps
789

790   **Fig. 9. Saturation indices of C_3S, CSH, and Portlandite**
791   Size: Single column
792   Filename: Figure 09 - Saturation Indices.eps
793

794   **Fig. 10. Weight losses (by % of original cement) as measured by TGA. Reported as**
795   **the total loss, loss associated with carbonates, total loss associated with bound water,**
796   **loss of bound water from C-S-H gel, and loss of bound water from portlandite**
797   Size: 1.5 columns
798   Filename: Figure 10 - C3S and Cement TGA.eps
799

800   **Fig. 11. SEM micrographs showing the formation of hydration products (with time)**
801   **in C_3S, control and CO_2 activated paste (Cc: Calcium carbonate; CH: Portlandite)**
802   Size: 1.5 columns
803   Filename: Figure 11 - C3S SEM comparison.tiff
804

805   **Fig. 12. EDS spectrum (left) of rhombohedral products observed in C_3S sample**
806   **activtated with CO_2 at 3 min (right). Analyzed particle indicated with an ×**
807   Size: 1.5 columns
808   Filename: Figure 12 - EDS spectra and SEM.tif

809
Fig. 13. SEM micrographs showing the formation of hydration products (with time)
in cement, control and CO₂ activated paste (Cc: Calcium carbonate; CH: Portlandite)

810

811

Size: 1.5 columns

812

Filename: Figure 13 - Cement SEM comparison.tiff

813

814